Case Studies in Construction Materials 16 (2022) e00927

Contents lists available at ScienceDirect

Case Studies in Construction Materials

journal homepage: www.elsevier.com/locate/cscm

Short communication

Effect of curing time on the chloride diffusion of alkali-activated slag

Antonino Runci, Marijana Serdar *

University of Zagreb, Faculty of Civil Engineering, Department of Materials, Croatia

ARTICLE INFO

Keywords:
Alkali activated slag
Chloride migration
Chloride diffusion
Pore structure
Electrical resistivity
Curing

ABSTRACT

Resistance to chloride penetration plays a crucial role in preventing premature corrosion of reinforced concrete in marine environments or when using de-icing salts. For reinforced concrete with ordinary Portland cement (OPC), the curing of concrete is vital in ensuring that the designed chloride penetration resistance of concrete is achieved. The method and duration of curing are especially important with alkali-activated slag (AAS) to allow proper reaction and development of the pore structure. AAS generally needs to be cured under closed conditions for at least 28 d to achieve the desired quality. The objective of this study was to analyse the effect of curing time on the development of chloride diffusion resistance and pore structure of alkali-activated slag mortar. Chloride diffusion resistance was analysed at 7, 28, and 90 d using non-steady-state chloride migration according to NT BUILD 492 and accelerated chloride testing according to NT BUILD 443, both of which were originally developed for OPC. Mercury intrusion porosimetry (MIP) was used to evaluate the effect of pore structure on chloride penetration. The diffusion results of alkali-activated mortar showed that high resistance to chlorides can be achieved after only 7 d of curing, which is attributed to the development of fine porosity of alkali-activated slag at an early age.

1. Introduction

Chloride penetration is a key parameter for determining the long-term durability of reinforced concrete. When chlorides penetrate the concrete and accumulate at the steel-concrete interface, corrosion of steel can be initiated, causing deterioration of the reinforced structure. Alkali-activated materials (AAMs) have already shown high resistance to chloride diffusion, mainly because of their porosity, pore structure, and chloride binding capacity. Ismail et al. [1] have demonstrated that binders based on alkali-activated slag have better resistance to chlorides than those based on alkali-activated fly ash, which was attributed to the calcium content in the precursor. The main reaction product of alkali-activated slag is C-A-S-H gel, which improves pore refinement [2]. Furthermore, slag generally requires a higher water-to-binder ratio than fly ash-based systems, and an increase in the water content leads to a decrease in the chloride diffusion resistance [3] while increasing the risk of drying shrinkage and cracking [4]. Regardless of the type of precursor used, increasing the alkali concentration (Na^+, K^+, Ca^{2+}) from the activators generally increases its dissolution, accelerates the geopolymerisation process, and results in a denser matrix, which improves the resistance to chloride penetration [3,5]. The silica modulus (Ms) is a parameter used in alkali-activated technology to determine the $SiO_2/(Na_2O + K_2O)$ ratio when a waterglass activator is used. A higher Ms value leads to an increase in the compressive strength and a decrease in the porosity and average pore size [6]. This

* Corresponding author.
E-mail address: marijana.serdar@grad.unizg.hr (M. Serdar).

https://doi.org/10.1016/j.cscm.2022.e00927
Received 30 September 2021; Received in revised form 17 January 2022; Accepted 2 February 2022

has a positive effect on the reduction of chloride diffusion. Ms is also responsible for improving the chloride-binding capacity [5,7]. AAMs generally provide lower porosity and smaller average pore radius than that of OPC, especially where C-A-S-H gel is the main reaction product owing to pore refinement [2,8]. Provis et al. [9] have shown that with an increase in curing time, the tortuosity increases and the overall permeability decreases, both of which strongly influence chloride diffusion [10]. Another important parameter is the chloride binding capacity, which is the ability of the reaction products to bind chloride anions from the pore solution into chemically bound hydrotalcite-like phases and physically adsorb chlorides on the C-A-S-H/N-A-S-H gel surface [11,12]. Unlike OPC, the absence of a specific reaction product that binds chloride anions (Friedel's salts) makes this property less stable and more variable in AAMs [12] because hydrotalcite and C-A-S-H/N-A-S-H gel are easily attacked by other aggressive agents such as atmospheric CO_2, acid attack, and leaching. Therefore, while carbonation and leaching play a minor role in Portland cement-based concretes, they can be a crucial aspect in AAMs, especially at early ages, reducing their resistance to chloride diffusion [13]. Owing to the absence of $Ca(OH)_2$, atmospheric CO_2 reacts with hydrotalcite and C-A-S-H/N-A-S-H gel, reducing the chloride binding capacity [12] and increasing porosity as a result of the formation of Na and Ca-carbonate and decomposition of gel and gel pores [14]. This can be intensified by a tendency to leach, especially with short curing times in fly ash-based systems, which are usually associated with a low degree of geopolymerisation [15] and/or the formation of efflorescence [16]. The curing method is an important parameter for the activation and development of the pore structure in AAM systems. Higher curing temperatures generally reduce the porosity and chloride penetration in AAMs, especially for fly ash-based systems [17]. Higher curing temperatures have also been shown to be beneficial in improving slag reactivity, which reduces porosity and chloride diffusion [18], even when curing in a conventional humidity chamber. However, the preferred curing method for alkali-activated slag remains dry curing, which ensures a system with better performance in terms of porosity and mechanical properties than that of conventional OPC [18,19]. Moreover, when cured under sealed conditions, the slag can react without water evaporation, avoid cracking and/or shrinkage, reduce possible pore structure changes, exhibit efflorescence due to the reaction of alkali with atmospheric CO_2, and leach under water exposure [4,8,14].

Other alternatives to OPC, such as binary and ternary blended cements made by CEM I and one or more supplementary cementitious materials (SCMs), often require prolonged curing times to ensure full hydration of systems and achieve properties comparable to those of OPC [20]. Indeed, the slower pozzolanic reaction of SCMs compared to the fast hydration of OPC can lead to poor performance of blended systems after a short curing time in terms of chloride penetration and carbonation [21,22]. Therefore, curing and testing after periods longer than 28 d are often recommended or requested for blended cements with low clinker content. Compared to OPC blended systems, AAMs can reach a high degree of reaction after only 24 h, which results in fine porosity and a sufficient amount of reaction products to protect the concrete from chloride diffusion [23]. This behaviour could be advantageous for the application of AAMs towards early age durability; however, there are no studies confirming that the degree of reaction after low curing times is sufficient to provide high chloride resistance. Most studies showed chloride diffusion properties after 28 d of curing [1–4] and eventually with prolonged exposure to NaCl solution [5]. Furthermore, there is no correlation with the pore structure, which can represent the crucial property to characterise the early age durability, unlike OPC and other binders [6].

The aim of this study is to evaluate the effect of curing time on the chloride diffusion/migration and porosity of mortar based on alkali-activated slag after different curing times. The significance of this study lies in the challenges that prolonged curing poses to the practical application of alkali-activated binders and the importance of ensuring adequate durability of alkali-activated slag exposed to the marine environment after a short curing period.

2. Materials and methods

2.1. Materials

Commercial ground granulated blast-furnace slag (BFS_E) supplied by Ecocem (Moerdijk, Netherlands) was used as a solid precursor for mortar preparation (mortar-labelled AAS). Blast furnace slag was activated by mixing the powder with 2.7 g of sodium silicate and 4 g of NaOH solution per 100 g of slag. The water-to-total solid mass ratio was 0.338. The activators used were sodium silicate Geosil 34417 from Woellner (Ludwigshafen am Rhein, Germany) with Ms = 1.68 and 12.5 M NaOH. Technical grade sodium hydroxide pellets supplied by Grammol (Zagreb, Croatia) were dissolved in distilled water and mixed to prepare NaOH solution (12.5 M) 24 h before mortar preparation to cool the alkaline solution. The test was performed at the mortar level with blast furnace slag to an aggregate mass ratio of 0.33. The aggregate used was local dolomite with 0–4 mm grain size.

2.2. Methods

The chemical composition of the slag was determined using X-ray fluorescence spectroscopy. The particle size distribution (PSD) was determined using a Mastersizer 2000 instrument (Malvern Panalytical, United Kingdom) with a wet laser diffraction procedure by dispersing the particles in isopropanol [9].

The slump of the mortar was measured using a flow table according to standard EN 1015–3. The air content was measured using pressure methods according to standard EN 1015–7. The slump and air content tests were conducted immediately after mixing under ambient conditions. The compressive strength was determined on three prisms of 4 × 4 × 16 cm per mix after 7 and 28 d with a loading rate of 2400 kN according to standard EN 196–1.

The resistance of alkali-activated mortar against chloride diffusion was measured by migration according to NT BUILD 497 and ponding according to NT BUILD 443. The fresh mortar was moulded into a ⌀100 × 200 mm cast cylinder. After 28 d of curing the surface electrical resistivity of the mortar was measured using the Wenner probe and then cut into three discs of ⌀100 × 50 mm,

eliminating the top and bottom of the cylinder.

The non-steady-state chloride migration was conducted on three specimens per mix after saturation with CaOH solution using a PROOVE'it instrument (Copenhagen, Denmark) with 0.3 N NaOH as the anolyte solution and 2 N NaCl as the catholyte solution. The test was carried out by applying a constant voltage of 30 V to the initial current. At the end of the test, the specimens were axially split and 0.1 M of $AgNO_3$ was sprayed on the fresh surface. The chloride penetration depth was measured from the white silver chloride precipitation (AgCl) when chloride is present in sufficient quantities (otherwise brown Ag_2O is precipitated), after which the chloride migration coefficient can be calculated using an integrated form of the Nernst–Planck equation:

$$\frac{D_{nssm} = 0.0239\bullet(273 + T\bullet L)}{(U-2)\bullet t\bullet\left(\mathrm{x_d} - 0.0238\bullet\sqrt{\frac{(237+\mathrm{T})\bullet \mathrm{L}\bullet \mathrm{x_d}}{\mathrm{U}-2}}\right)} \tag{1}$$

where D_{nssm} is the chloride migration coefficient in $\times 10^{-12}$ m^2/s, U is the applied voltage in V, T is the average of the initial and final temperatures in °C, L is the thickness of the sample in mm, x_d is the average penetration depth in mm, and t is the test duration in h. An important parameter for this test is the chloride concentration at which the colour changes (c_d). The NT BUILD 492 recommends a c_d value of 0.07 N for OPC concrete. However, for AAMs, $c_d = 0.21$ was applied [1,15] to consider hydroxide ions (pH value). In fact, silver nitrate can react with both chloride ions and hydroxyl ions to form white silver chloride (AgCl) and dark brown silver oxide (Ag_2O). When an aqueous silver nitrate solution is sprayed on the surface of the split concrete, the precipitates formed on the surface of the concrete are a mixture of AgCl and Ag_2O. For each chemistry of the pore solution, there is a critical point where the brown colour of the silver oxide covers the white colour of the silver chloride and forms the penetration front. The concentration of chloride ions at this critical point (penetration front) is taken as c_d. The silver nitrate colorimetric measurement is based on a chemical reaction, which might be influenced by the chemistry of the concrete pore solution. The fact that alkali-activated materials have a different pore solution chemistry, which is not considered in the NT BUILD 492 method, is accommodated by a difference in the c_d parameter.

Bulk diffusion testing was performed on three specimens per mix. Prior to ponding, the samples were saturated with $Ca(OH)_2$ solution and coated with a thin epoxy layer, leaving one face free to allow the ingress of unidimensional chloride. The prepared samples were immersed in a 16 g/L NaCl solution. After 45 days of exposure, grinding was performed with a Germann Instruments Profile Grinder (Copenhagen, Denmark). From the sample powder extracted at different depths, the total chloride (acid-soluble) was calculated to estimate the apparent chloride diffusion coefficient (D_a) as the average of two specimens per mix. Additionally, the pH was measured to evaluate the leaching effect.

The total chloride content was measured according to EN 14629 [24]. Five grams of powder was dissolved in 100 ml of distilled water and stirred to remove any lumps. Then, 10 ml of 5 M HNO_3 acid solution and 4 drops of H_2O_2 (to avoid reduced sulphur contribution) were added and continuously stirred and heated until boiling. The total chloride content was measured by 0.1 M $AgNO_3$ titration using a TitroLine 5000 (SI Analytics) with the equivalent point methods. The chloride content was calculated using Eq. 2:

$$\frac{Cl, \quad \% = 3.545\bullet[(V_1 - V_2)\bullet N]}{W} \tag{2}$$

where V_1 is the volume of 0.1 N $AgNO_3$ solution used for sample titration in ml, V_2 is the volume of 0.1 N $AgNO_3$ solution used for blank titration in ml, N is the exact normality of 0.1 N $AgNO_3$ solution, and W is the mass of sample in g. The chloride profile of each concrete sample was plotted to determine the apparent chloride diffusion coefficient. The apparent chloride diffusion was obtained by fitting Eq. (3) to the plotted chloride profile by means of nonlinear regression analysis using the least squares method.

$$C(x,t) = C_s - (C_s - C_i)\bullet\mathrm{erf}\left(\frac{\mathrm{x}}{\sqrt{4\bullet \mathrm{D_a}\bullet \mathrm{t}}}\right) \tag{3}$$

where C(x,t) is the chloride concentration measured at depth x and exposure time t in mass %, C_s is the chloride concentration at the exposure surface (boundary condition), which is determined by the regression analysis in mass %, C_i is the initial chloride concentration of the concrete sample at time $t = 0$ in mass %, x is the depth below the exposed surface in m, t is the exposure time in s, D_a is the apparent diffusion coefficient in m^2/s, and erf denotes the error function described in Eq. (4).

$$erf(z) = \frac{2}{\pi}\int_0^z exp(-u^2)du \tag{4}$$

The pH was measured by dissolving 3 g of the powder in 30 ml of distilled water. The solution was stirred in the first 5 min, then stored at 20 ± 1 °C for 24 h. Subsequently, it was vacuum filtered using Ahlstrom-Munksjö (Helsinki, Finland) filter paper with a pore size of 2–3 μm in a Buchner funnel and suctioned filtration flask. The pH of the obtained leachate solution was deemed to be an acceptable approximation of the pH of the mortar pore solution [25]. The pH was measured using a Lab 850 SCHOOTT Instrument (Hattenbergstr, Germany).

Mercury intrusion porosimetry (MIP) was used to provide information regarding the pore size distribution and pore volume of the mortars in the range 0.006–360 μm. The specimens for MIP were crushed into small pieces and immersed in isopropanol 7 d after they were vacuum dried. Autopore IV 9505 was used for MIP measurements, with a maximum pressure of 208 MPa. The pore diameter was derived using Washburn's law, given by:

$$D = \frac{(-4\cos\theta)\bullet\gamma}{P} \quad (5)$$

where D is the pore diameter (μm), θ is the contact angle between the fluid and the pore mouth (130°), γ is the surface tension of the fluid (485 mN/m), and P is the applied pressure to fill the pores with mercury (MPa). The total porosity was quantified by dividing the total intruded Hg (ml) by the sample weight (g). The critical pore entry radius, r_{crit}, was mathematically obtained from the maximum derivative of the pore entry radius distribution, calculated as the inflexion point of the main intrusion step, and is the pore size where the steepest slope of the cumulative intrusion curve is recorded [26].

3. Results and discussion

Table 1 lists the chemical composition of the blast furnace slag in the oxides. Blast furnace slag is rich in hydraulic oxides, contributing to its high reactivity with SCM. Fig. 1 shows the particle size distributions of blast furnace slag, which has very fine particles with a bulk particle size of approximately 10 μm, with a median d_{50} of 4.9 μm. The fineness of the slag accelerates its dissolution and geopolymerisation process with the alkali activator solution, further increasing the compressive strength and decreasing the porosity; consequently, chloride penetration can be reduced [7,8]. The particle density was 2.89 g/cm^3.

After mixing, the fresh properties of the AAMs were tested as described in the Methods section. The alkali-activated slag (AAS) mortar shows a consistency of 160 mm and an air content of 4.3%. Fig. 2 shows the mechanical properties of AAS after 7 and 28 d of curing under sealed conditions. Despite being at the mortar level, the compressive strength obtained is comparable with that of S3 from RILEM TC-247 [27] on the concrete level.

The total chloride content (a) and pH profiles (b) of AAS after different curing times (7, 28, and 90 d) exposed to a 16.5% NaCl solution for 45 days are shown in Fig. 3. Based on the pH values before immersion, a decrease was observed from 12.8 after 7 days to 12.3 after 90 days of curing. This decrease in pH was evident despite the sealed conditions during curing, indicating the consumption of OH^- anions for dissolving aluminosilicate powder and a continuous reaction even after 90 d [28]. However, once the samples were exposed to a chloride solution, longer curing times provided a more stable pH, suggesting that longer curing leads to a lower risk of paste leaching during exposure. After 7 d, the pH decreased sharply at the shallow depth of the samples and stabilised at 8 mm, whereas after 28 and 90 d of curing, the pH slowly increased at a depth of 4 mm, reaching a value similar to the initial value after 7 d of curing. Contrary to what has been reported in the literature [3], there is no visible correlation between the pH and the diffusion of Cl^- anions at the studied depth. The lack of correlation between chloride and pH profiles is probably due to the low exposure time and the fine porosity of AAS [3].

Table 2 shows the chloride migration coefficient (D_{nnssm}) tested according to standard NT BUILD 492 and summarises the parameters for calculating the apparent chloride diffusion coefficient (D_a) according to standard NT BUILD 443. The results show that as the curing time increased, the chloride diffusion coefficient decreased, and the surface resistivity increased. Chloride penetration decreased with an increase in curing time; however, the decrease was not as steep as previously described [1,29]. Furthermore, despite the short curing time, 7 d were sufficient for developing high resistance to chloride penetration. In contrast, most binary and/or ternary cementitious mixtures do not provide sufficient protection against the diffusion of Cl^- anions at short curing times and therefore require long-term curing to compete with OPC [21,22,30]. This is attributed to the fact that the hydration reaction takes longer because of the lower pH of the pore solution [31,32]. On the other hand, the high alkalinity of the activator early in the process is sufficient to dissolve and polymerise the blast furnace slag rapidly, ensuring a high reaction level after 28 d, especially in the presence of waterglass [23,31].

The two accelerated tests showed a similar trend. The chloride migration coefficient (D_{nnssm}) and the apparent chloride diffusion coefficient (D_a) have a coefficient of correlation r = 0.9 (Fig. 4). Therefore, the NT BUILD 492 chloride migration test method can be used to assess the chloride penetration resistivity of alkali-activated slag. Similarly, apparent chloride diffusion and surface resistivity are also in good correlation, with a coefficient of correlation r = 0.97 (Fig. 4).

The low chloride penetration in alkali-activated slag is usually attributed to the microstructure of the mortar and the chloride binding capacity [7,11]. Fig. 5 shows the cumulative pore curve (a) and the pore size differential curve (b) for AAS cured for 7, 28, and 90 d. As the curing time increased from 7 to 28 d, the shape of the cumulative curve did not change significantly. After 90 d, AAS had extremely low porosity, and most pores were not accessible to Hg. With longer curing time, the slag had more time to react, and the amount of precipitated C-A-S-H gel increased. Moreover, with longer curing time, the number of accessible capillary pores decreased, and the number of gel pores increased [23], supporting the sealed conditions [33].

The porosity decreased significantly as the samples matured, as can be seen in Table 3. Such a significant decrease in pore structure can be attributed to the composition of the activator and the Ms of the waterglass used in the system, which provides a more homogenous and denser matrix and a higher degree of reaction than systems based only on NaOH [23]. Nevertheless, a significant reduction in porosity did not significantly affect the chloride penetration. This is because the chloride penetration is mainly influenced

Table 1
Chemical composition of blast furnace slag.

Oxide composition (mass %)									
SiO_2	Al_2O_3	Fe_2O_3	MnO	TiO_2	CaO	MgO	K_2O	Na_2O	SO_3
31.1	13.7	0.401	0.31	1.26	40.9	9.16	0.68	0	2.31

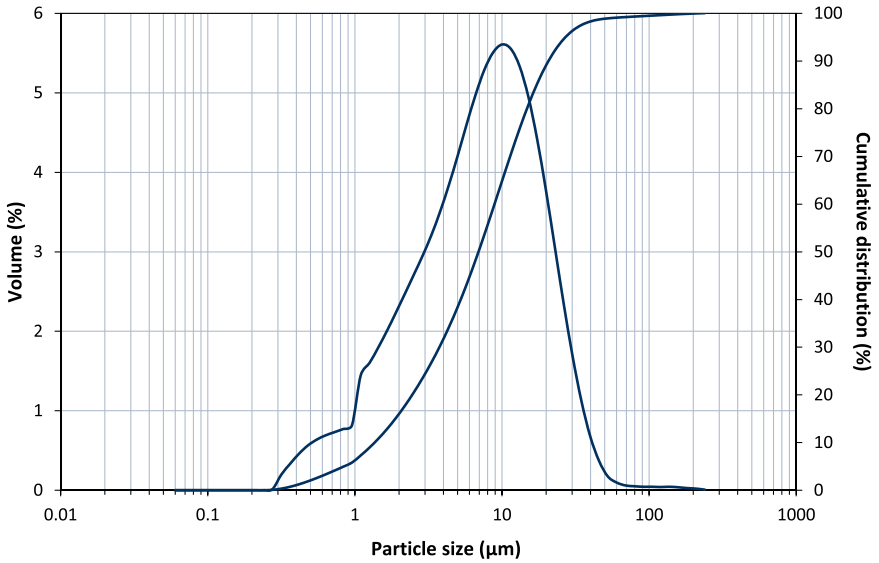

Fig. 1. Particle size distribution (PSD) of blast furnace slag from laser diffraction.

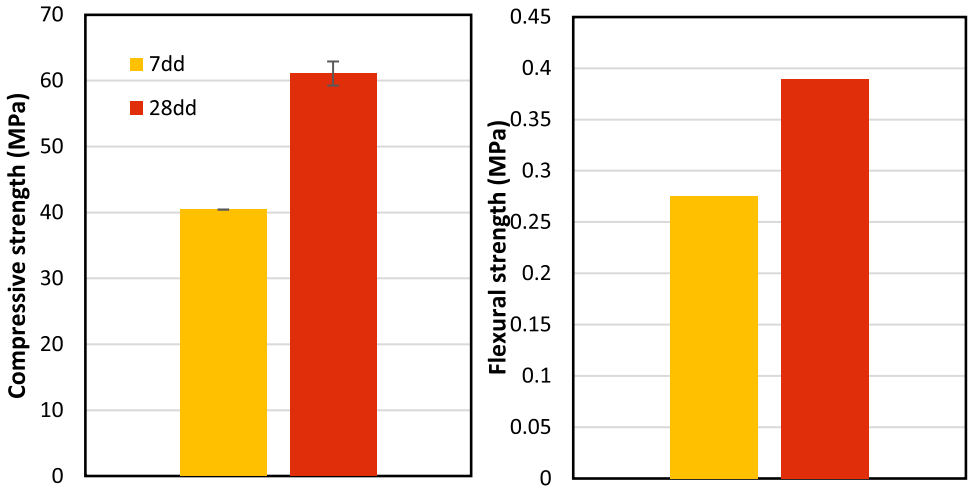

Fig. 2. Compressive and flexural strength of AAS after 7 and 28 d of curing.

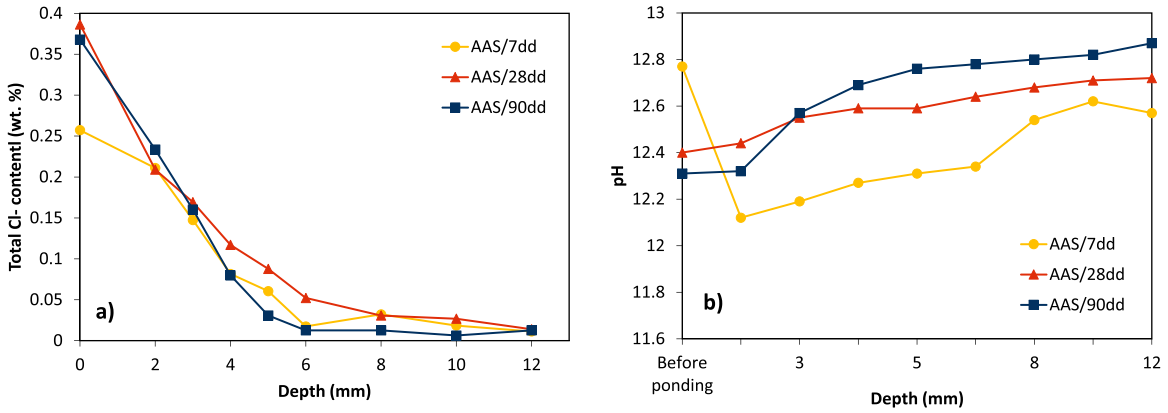

Fig. 3. Total chloride (a) and pH profile (b) after 45 days of ponding of AAS mortar cured for 7, 28 and 90 d.

Table 2
Chloride migration and apparent chloride diffusion coefficients of AAS.

Curing (d)	D_{nnssm} (x 10^{-12} m^2/s)	D_a (x 10^{-12} m^2/s)	C_s (mass %)	C_i (mass%)	SSE[a]
7	2.3 ± 0.16	2 ± 0.2	0.273	0.01	0.001
28	2.06 ± 0.36	1.6 ± 0.1	0.421	0.01	0.0003
90	1.62 ± 0.49	1.3 ± 0.13	0.394	0.01	0.001

[a] sum of square errors

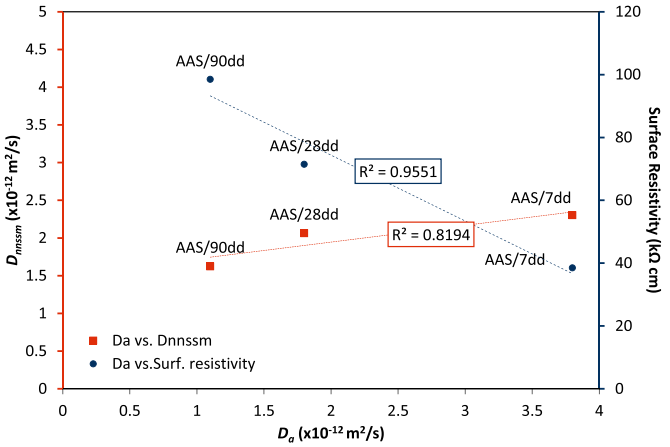

Fig. 4. Apparent chloride diffusion coefficient vs. non-steady state chloride migration coefficient and surface resistivity of AAS mortar cured for 7, 28 and 90 d.

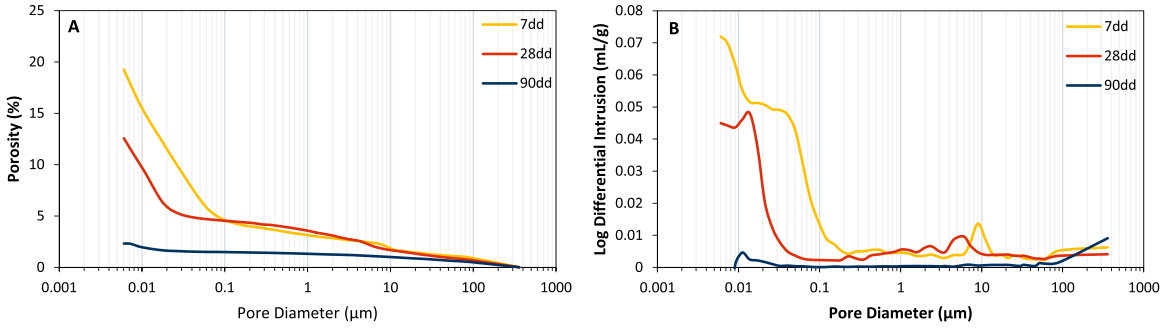

Fig. 5. Pore size distribution (a) cumulative curve and (b) differential curve of AAS mortar cured for 7, 28 and 90 d.

Table 3
Porosity characteristics of AAS mortar cured for 7, 28 and 90 d.

Curing (d)	Total Porosity (%)	Critical pore radius entry (μm)	Gel pores (%) < 0.015 μm	Capillary pores (%) 0.015–1 μm
7	19.25	0.05649	5.65	9.15
28	12.56	0.01908	4.80	3.25
90	2.3	0.00815	0.55	0.33

by the capillary pore region (0.015–1 μm) and partially by macropores [34,35]. AAS has shown finer porosity than OPC after 28 d of curing [36]. Many binary and ternary blended cements from the literature [37,38] showed greater overall porosity than OPC at early stages and required a long curing time to achieve comparable results, whereas AAS already showed fine porosity and excellent resistance to chloride ingress after 7 d of curing.

Fig. 6 shows the correlation between the chloride diffusion coefficient and total and capillary pore volume (in red) and the critical pore radius entry (in blue). The mortars showed a strong correlation between the apparent chloride diffusion coefficient and the pores in the capillary size range, with a correlation coefficient of 0.994. The correlations between porosity and apparent chloride diffusion have not yet been observed for AAMs [36,39,40]. Furthermore, the graph displays a strong correlation with a coefficient of correlation

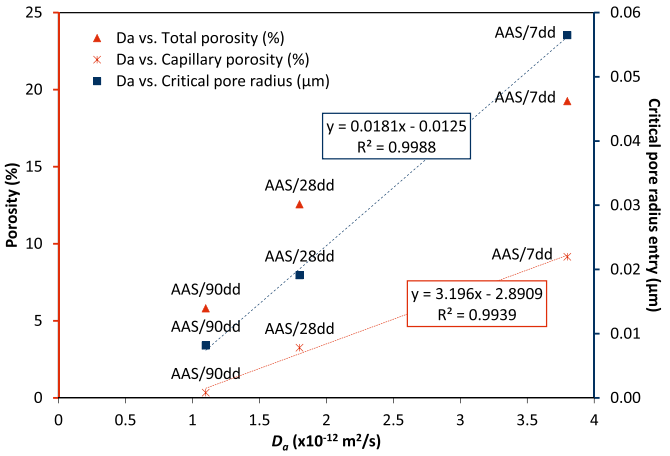

Fig. 6. Apparent chloride diffusion coefficient vs. total porosity, capillary porosity (0.015–1 μm) and critical pore radius entry for AAS mortar cured for 7, 28 and 90 d.(For interpretation of the references to colour in this figure, the reader is referred to the web version of this article.)

of 0.99, as has been previously shown for blended cements [30]. However, the relationship between the total porosity and curing time is not linear.

After a certain critical pore radius entry, r_{crit}, was reached, the apparent chloride diffusion coefficient was extremely low. This very low chloride diffusion in AAS at early and later stages can be attributed to two crucial properties: i) tortuosity [9], τ, and ii) chloride binding capacity [11]. Provis et al. [9] demonstrated a marked increase in of tortuosity in alkali-activated slag in the early reaction phase, with an overall inverse relationship with porosity [41]. A longer curing time contributes to a higher degree of reaction, which is a crucial variable for the chloride binding capacity, P_{bc}. In AAS, Cl^- anions are chemically bound to hydrotalcite and physically adsorbed on the C-A-S-H gel surface [11,12], greatly reducing the chloride diffusion coefficient [3].

4. Conclusion

In a conventional OPC system, especially in blended cementitious systems, the curing duration plays a crucial role in ensuring that the system achieves its designed properties. In the present study, the chloride diffusion resistance and the pore structure of alkali-activated slag were analysed after 7, 28, and 90 d of curing to understand its effects on chloride diffusion resistance.

The results show that AAS has a high resistance to chloride penetration even after a short curing time. There is a strong correlation between the resistance of AAS to chloride penetration and the porosity in the capillary size region and the critical pore radius. The maturation (curing duration) of the alkali-activated slag significantly affected the overall porosity but did not result in a further decrease in the chloride penetration resistance. The fact that AAS achieved a very low chloride diffusion coefficient after only 7 d is advantageous for its application in marine environments, giving it an edge over other OPC alternatives.

Future research should focus more precisely on distinguishing the influence of chloride binding capacity from porosity on the chloride diffusion coefficient and consider a wider range of mixture designs.

Declaration of Competing Interest

The authors declare that they have no known competing financial interests or personal relationships that could have appeared to influence the work reported in this paper.

Acknowledgment

Research presented in this paper was performed within project DuRSAAM, which has received funding from the European Union's Horizon 2020 research and innovation programme under grant agreement No 813596. Research is also supported by the project "Alternative Binders for Concrete: understanding microstructure to predict durability, ABC", funded by the Croatian Science Foundation under number UIP-05-2017-4767.

References

[1] I. Ismail, S.A. Bernal, J.L. Provis, R. San Nicolas, D.G. Brice, A.R. Kilcullen, S. Hamdan, J.S.J. Van Deventer, Influence of fly ash on the water and chloride permeability of alkali-activated slag mortars and concretes, Constr. Build. Mater. 48 (2013) 1187–1201, https://doi.org/10.1016/j.conbuildmat.2013.07.106.
[2] M. Babaee, A. Castel, Water vapor sorption isotherms, pore structure, and moisture transport characteristics of alkali-activated and Portland cement-based binders, Cem. Concr. Res. 113 (2018) 99–120, https://doi.org/10.1016/j.cemconres.2018.07.006.
[3] D. Bondar, Q. Ma, M. Soutsos, M. Basheer, J.L. Provis, S. Nanukuttan, Alkali activated slag concretes designed for a desired slump, strength and chloride diffusivity, Constr. Build. Mater. 190 (2018) 191–199, https://doi.org/10.1016/j.conbuildmat.2018.09.124.

[4] N.K. Lee, J.G. Jang, H.K. Lee, Shrinkage characteristics of alkali-activated fly ash/slag paste and mortar at early ages, Cem. Concr. Compos. 53 (2014) 239–248, https://doi.org/10.1016/j.cemconcomp.2014.07.007.
[5] Q. Ma, S.V. Nanukuttan, P.A.M. Basheer, Y. Bai, C. Yang, Chloride transport and the resulting corrosion of steel bars in alkali activated slag concretes, Mater. Struct. Mater. Et. Constr. 49 (2016) 3663–3677, https://doi.org/10.1617/s11527-015-0747-7.
[6] S. Fang, E.S.S. Lam, B. Li, B. Wu, Effect of alkali contents, moduli and curing time on engineering properties of alkali activated slag, Constr. Build. Mater. 249 (2020), 118799, https://doi.org/10.1016/j.conbuildmat.2020.118799.
[7] H. Ye, L. Huang, Z. Chen, Influence of activator composition on the chloride binding capacity of alkali-activated slag, Cem. Concr. Compos. 104 (2019), 103368, https://doi.org/10.1016/j.cemconcomp.2019.103368.
[8] N.K. Lee, H.K. Lee, Setting and mechanical properties of alkali-activated fly ash/slag concrete manufactured at room temperature, Constr. Build. Mater. 47 (2013) 1201–1209, https://doi.org/10.1016/j.conbuildmat.2013.05.107.
[9] J.L. Provis, R.J. Myers, C.E. White, V. Rose, J.S.J.Van Deventer, X-ray microtomography shows pore structure and tortuosity in alkali-activated binders, Cem. Concr. Res. 42 (2012) 855–864, https://doi.org/10.1016/j.cemconres.2012.03.004.
[10] M.A.B. Promentilla, S.M. Cortez, R.A.D.C. Papel, B.M. Tablada, T. Sugiyama, Evaluation of microstructure and transport properties of deteriorated cementitious materials from their X-ray computed tomography (CT) images, Materials 9 (2016), https://doi.org/10.3390/ma9050388.
[11] J. Zhang, C. Shi, Z. Zhang, Chloride binding of alkali-activated slag/fly ash cements, Constr. Build. Mater. 226 (2019) 21–31, https://doi.org/10.1016/j.conbuildmat.2019.07.281.
[12] X. Ke, S.A. Bernal, J.L. Provis, Uptake of chloride and carbonate by Mg-Al and Ca-Al layered double hydroxides in simulated pore solutions of alkali-activated slag cement, Cem. Concr. Res. 100 (2017) 1–13, https://doi.org/10.1016/j.cemconres.2017.05.015.
[13] S.A. Bernal, R. Mejía De Gutiérrez, J.L. Provis, Engineering and durability properties of concretes based on alkali-activated granulated blast furnace slag/metakaolin blends, Constr. Build. Mater. 33 (2012) 99–108, https://doi.org/10.1016/j.conbuildmat.2012.01.017.
[14] S.A. Bernal, J.L. Provis, Durability of alkali-activated materials: progress and perspectives, J. Am. Ceram. Soc. 97 (2014) 997–1008, https://doi.org/10.1111/jace.12831.
[15] A. Noushini, A. Castel, J. Aldred, A. Rawal, Chloride diffusion resistance and chloride binding capacity of fly ash-based geopolymer concrete, Cem. Concr. Compos. (2019), 103290, https://doi.org/10.1016/j.cemconcomp.2019.04.006.
[16] M. Dong, M. Elchalakani, A. Karrech, Curing conditions of alkali-activated fly ash and slag mortar, J. Mater. Civ. Eng. 32 (2020), 04020122, https://doi.org/10.1061/(asce)mt.1943-5533.0003233.
[17] A. Noushini, A. Castel, The effect of heat-curing on transport properties of low-calcium fly ash-based geopolymer concrete, Constr. Build. Mater. 112 (2016) 464–477, https://doi.org/10.1016/j.conbuildmat.2016.02.210.
[18] M. Chi, Effects of dosage of alkali-activated solution and curing conditions on the properties and durability of alkali-activated slag concrete, Constr. Build. Mater. 35 (2012) 240–245, https://doi.org/10.1016/j.conbuildmat.2012.04.005.
[19] Y.R. Alharbi, A.A. Abadel, A.A. Salah, O.A. Mayhoub, M. Kohail, Engineering properties of alkali activated materials reactive powder concrete, Constr. Build. Mater. 271 (2021), 121550, https://doi.org/10.1016/j.conbuildmat.2020.121550.
[20] W. Wilson, F. Georget, K. Scrivener, Unravelling chloride transport/microstructure relationships for blended-cement pastes with the mini-migration method, Cem. Concr. Res. 140 (2021), 106264, https://doi.org/10.1016/j.cemconres.2020.106264.
[21] Q.D. Nguyen, S. Afroz, A. Castel, Influence of calcined clay reactivity on the mechanical properties and chloride diffusion resistance of limestone calcined clay cement (LC3) concrete, J. Mar. Sci. Eng. 8 (2020) 1–14.
[22] V. Elfmarkova, P. Spiesz, H.J.H. Brouwers, Determination of the chloride diffusion coefficient in blended cement mortars, Cem. Concr. Res. 78 (2015) 190–199, https://doi.org/10.1016/j.cemconres.2015.06.014.
[23] M. Ben Haha, G. Le Saout, F. Winnefeld, B. Lothenbach, Influence of activator type on hydration kinetics, hydrate assemblage and microstructural development of alkali activated blast-furnace slags, Cem. Concr. Res. 41 (2011) 301–310, https://doi.org/10.1016/j.cemconres.2010.11.016.
[24] BS EN 14629, Products and systems for the protection and repair of concrete structures - test methods - determination of chloride content in hardened concrete, Br. Stand. 3 (2007).
[25] V. Räsänen, V. Penttala, The pH measurement of concrete and smoothing mortar using a concrete powder suspension, Cem. Concr. Res. 34 (2004) 813–820, https://doi.org/10.1016/j.cemconres.2003.09.017.
[26] K. Scrivener, R. Snellings, B. Lothenbach. A Practical Guide to Microstructural Analysis of Cementitious Materials, CRC Press, 2015, https://doi.org/10.1201/b19074.
[27] J.L. Provis, K. Arbi, S.A. Bernal, D. Bondar, A. Buchwald, A. Castel, S. Chithiraputhiran, M. Cyr, A. Dehghan, K. Dombrowski-Daube, A. Dubey, V. Ducman, G.J.G. Gluth, S. Nanukuttan, K. Peterson, F. Puertas, A. van Riessen, M. Torres-Carrasco, G. Ye, Y. Zuo, RILEM TC 247-DTA round robin test: mix design and reproducibility of compressive strength of alkali-activated concretes, Mater. Struct. 52 (2019) 1–13, https://doi.org/10.1617/s11527-019-1396-z.
[28] S.A. Bernal, J.L. Provis, B. Walkley, R. San Nicolas, J.D. Gehman, D.G. Brice, A.R. Kilcullen, P. Duxson, J.S.J.Van Deventer, Gel nanostructure in alkali-activated binders based on slag and fly ash, and effects of accelerated carbonation, Cem. Concr. Res. 53 (2013) 127–144, https://doi.org/10.1016/j.cemconres.2013.06.007.
[29] M. Criado, S.A. Bernal, P. Garcia-Triñanes, J.L. Provis, Influence of slag composition on the stability of steel in alkali-activated cementitious materials, J. Mater. Sci. 53 (2018) 5016–5035, https://doi.org/10.1007/s10853-017-1919-3.
[30] S. Sui, F. Georget, H. Maraghechi, W. Sun, K. Scrivener, Towards a generic approach to durability: factors affecting chloride transport in binary and ternary cementitious materials, Cem. Concr. Res. 124 (2019), 105783, https://doi.org/10.1016/j.cemconres.2019.105783.
[31] A. Gruskovnjak, B. Lothenbach, L. Holzer, R. Figi, F. Winnefeld, Hydration of alkali-activated slag: comparison with ordinary portland cement, Adv. Cem. Res. 18 (2006) 119–128, https://doi.org/10.1680/adcr.2006.18.3.119.
[32] A. Vollpracht, B. Lothenbach, R. Snellings, J. Haufe, The pore solution of blended cements: a review, Mater. Struct. /Mater. Et. Constr. 49 (2016) 3341–3367, https://doi.org/10.1617/s11527-015-0724-1.
[33] T. Yang, X. Yao, Z. Zhang, Quantification of chloride diffusion in fly ash-slag-based geopolymers by X-ray fluorescence (XRF), Constr. Build. Mater. 69 (2014) 109–115, https://doi.org/10.1016/j.conbuildmat.2014.07.031.
[34] R. Kumar, B. Bhattacharjee, Porosity, pore size distribution and in situ strength of concrete, Cem. Concr. Res. 33 (2003) 155–164, https://doi.org/10.1016/S0008-8846(02)00942-0.
[35] P.K. Mehta, P.J.M. Monteiro, Concrete Microstructure, Properties, and Materials, 2006.
[36] A. Runci, M. Serdar, Chloride-induced corrosion of steel in alkali-activated mortars based on different precursors, Materials 13 (5244) (2020) 1–17, https://doi.org/10.3390/ma13225244.
[37] Q. Zeng, K. Li, T. Fen-Chong, P. Dangla, Analysis of pore structure, contact angle and pore entrapment of blended cement pastes from mercury porosimetry data, Cem. Concr. Compos. 34 (2012) 1053–1060, https://doi.org/10.1016/j.cemconcomp.2012.06.005.
[38] Y. Jeong, H. Park, Y. Jun, J.H. Jeong, J.E. Oh, Microstructural verification of the strength performance of ternary blended cement systems with high volumes of fly ash and GGBFS, Constr. Build. Mater. 95 (2015) 96–107, https://doi.org/10.1016/j.conbuildmat.2015.07.158.
[39] C. Monticelli, M.E. Natali, A. Balbo, C. Chiavari, F. Zanotto, S. Manzi, M.C. Bignozzi, A study on the corrosion of reinforcing bars in alkali-activated fly ash mortars under wet and dry exposures to chloride solutions, Cem. Concr. Res. 87 (2016) 53–63, https://doi.org/10.1016/j.cemconres.2016.05.010.
[40] H. Zhu, Z. Zhang, Y. Zhu, L. Tian, Durability of alkali-activated fly ash concrete: chloride penetration in pastes and mortars, Constr. Build. Mater. 65 (2014) 51–59, https://doi.org/10.1016/j.conbuildmat.2014.04.110.
[41] M.A.B. Promentilla, T. Sugiyama, T. Hitomi, N. Takeda, Quantification of tortuosity in hardened cement pastes using synchrotron-based X-ray computed microtomography, Cem. Concr. Res. 39 (2009) 548–557, https://doi.org/10.1016/j.cemconres.2009.03.005.